Materials Science & Engineering A 650 (2016) 497–509

Contents lists available at ScienceDirect

Materials Science & Engineering A

journal homepage: www.elsevier.com/locate/msea

The effect of loading direction and Sn alloying on the deformation modes of Zr: An in-situ neutron diffraction study

K.V. Mani Krishna [a], D.G. Leo Prakash [b,c], Gábor Timár [b], Arnas Fitzner [b], D. Srivastava [a], N. Saibaba [d], J. Quinta da Fonseca [b], G.K. Dey [a], M. Preuss [b,*]

[a] Materials Science Division, Bhabha Atomic Research Centre, Trombay, Mumbai, India
[b] Manchester Materials Science Centre, The University of Manchester, Grosvenor Street, Manchester M1 7HS, UK
[c] Materials Research Centre, College of Engineering, University of Swansea, Swansea SA2 8PP, UK
[d] Nuclear Fuel Complex, Hyderabad, India

ARTICLE INFO

Article history:
Received 5 August 2015
Received in revised form
12 October 2015
Accepted 13 October 2015
Available online 11 November 2015

Keywords:
Neutron scattering
Plasticity
Twinning zirconium

ABSTRACT

Deformation modes (slip and twining) in a strongly textured model hcp alloy system (Zr–Sn) have been investigated using in-situ neutron diffraction and deformation along with complementary electron microscopy. Analysis of the evolution of the intergranular strain evolutions and intensity of specific reflections from neutron diffraction show differential influence of Sn on the extent of twinning too, depending on the deformation direction. While Sn displayed very noticeable influence on twin activity when samples were compressed along a direction that predominantly activates prismatic slip, this effect was not seen when samples were compressed along other different directions. These experimental observations were successfully simulated using a CPFE (crystal plasticity finite element) model that incorporates composition sensitive CRSS (critical resolved shear stress) for slip and composition insensitive CRSS activation of twinning. The success of the CPFE model in capturing the experimental observations with respect to twin evolution suggests that the twinning in Zr is chiefly governed by the initial crystallographic texture and the associated intergranular stress state generated during plastic deformation.

1. Introduction

Slip and twinning are two principal modes of plastic deformation in metallic materials [1,2]. It is well known that slip by dislocations contributes to the majority of observed deformation. Twinning on the other hand, results in significant changes in the crystal orientation and consequent crystallographic texture evolution [3–5]. Thus understanding of both of these phenomena is essential for deciphering plastic deformation and associated microstructural and textural evolutions. Although the existing knowledge on the mechanisms of slip in cubic materials is quite extensive, the same cannot be said for hexagonal close packed (hcp) materials. This is partly due to the interplay of multiple slip systems that makes the deformation a more complicated process [6,7]. The role of alloying elements on the deformation modes in these materials further complicates the picture. In addition to complications due to multiple slip modes, hcp materials are also known for their extensive tendency for twinning on account of paucity of easy slip systems along certain crystallographic directions [1,8–10]. Twinning in these materials plays a crucial role in textural evolution and low temperature ductility. Thus, our ability to develop predictive deformation models for hcp materials critically depend on understanding the role of alloying elements on these two different modes of deformation, i.e. slip and twinning.

Due to significant differences in the core structures of dislocations belonging to different slip modes (for e.g. $<a>$ type and $<c+a>$ type dislocations) [11,12], *prima facie* it appears that the influence of the alloying element shall be different in these slip modes. However, such effects are not documented in the available literature. Further, the mechanism and criteria under which deformation twins form and grow are not fully understood. Again, the role of alloying elements in deformation twinning adds additional complexity. Presently, there is no concrete experimental evidence of the governing criteria for the twin nucleation and previous work has relied chiefly on model assumptions. Some studies have considered the formation of mechanical twins to be primarily stress driven [4,13], while others indicate that twin nucleation is governed by the density and type of dislocation structure. For instance, there is considerable evidence to show that the twinning dislocations are a result of non planar dissociation reactions from $<a>$, $<c+a>$, and $<c>$ type dislocations [14–18]. Since dislocation structure and its distribution are mainly

* Corresponding author.
E-mail address: michael.preuss@manchester.ac.uk (M. Preuss).

http://dx.doi.org/10.1016/j.msea.2015.10.047

influenced by the plastic strain in the grains, twinning can potentially depend on the strain undergone by the parent grains as well. This raises the fundamental question of whether twinning is controlled by stress level, amount of plastic strain, or a combination of both. This is an important consideration for being able to model the deformation behaviour of the hcp materials.

The present study aims at providing answers to these questions by using in-situ neutron diffraction experiments on the deformation of four different Zr–Sn binary alloys. By generating comparable starting microstructures and textures in those binary alloys and compressing them along the three principle directions of the rolled plate, it was possible to preferentially activate different deformation modes and monitor the related twin formation and evolution during in-situ compression using time-of-flight neutron diffraction. Due to the in-situ nature of the experiments, and the arrangement of the detector banks, it was possible to measure the elastic strains and observe trends in peak broadening of grain families that tend to twin. In addition, the change in intensity of specific reflections can be used to detect the onset and subsequent evolution of twinning. A comprehensive analysis of this data is presented together with results from a crystal plasticity finite element model (CPFEM). The CPFEM accounts for the various slip modes and invokes twinning based on a critical resolved shear stress criterion. The principle idea of using the CPFEM in the present work is to replicate the observations obtained during the in-situ loading experiments and determine to what extent a CRSS based model can predict the onset and evolution of twinning measured experimentally. Although the material studied is a Zr alloy, our findings are relevant to the deformation of other hcp materials like Mg and Ti. It may be acknowledged that the role of an alloying element (Zn) on different deformation modes in case of another hcp metal, i.e., Mg has been investigated by Stanford et al. [19]. However, it may be noted that the concerned investigation employed the flow behaviour and pre and post texture data for interpretation of the results. Present work on the other hand made use of intergranualr strain evolutions across different grain families using in-situ deformation coupled with CPFE model incorporating twining to bring out the role of Sn on deformation of Zr.

2. Experimental and simulation methods

2.1. Material and processing of samples

Four model Zr–Sn binary alloys with nominal compositions of 0.15%, 0.23%, 0.33%, and 1.20% Sn (amounts are in weight percentage), were used in the present study (see Table 1, for detailed composition). More compositions were deliberately chosen towards a lower Sn content, instead of using equal steps of Sn variation. All alloys were prepared using a single batch of Zr sponge to minimize variation in trace elements. A detailed description of the preparation and thermo mechanical processing of the alloy samples can be found elsewhere [20]. For the sake of completeness a brief account of pre-processing of the samples is presented here.

Table 1
Composition of the Zr–Sn binary alloys used in the present study.

	Designation in the manuscript	Elements				
		Sn (wt%)	O (ppm)	C (ppm)	N (ppm)	Zr
Alloy 1	0.15% Sn	0.15	530	80	48	Balance
Alloy 2	0.23% Sn	0.23	880	80	45	Balance
Alloy 3	0.33% Sn	0.33	830	30	49	Balance
Alloy 4	1.20% Sn	1.20	930	120	34	Balance

The cast ingots were subjected to hot extrusion (at 800 °C) followed by β quenching treatment (at 1050 °C). While extrusion resulted in breaking of cast structure, β treatment was helpful in improving chemical homogeneity. Subsequently, one more homogenization treatment at 550 °C for 24 h, followed by slow cooling, was also performed. These homogenized samples were finally subjected to hot rolling for 65% reduction and annealing treatment. Both of these treatments were performed at 550 °C followed by a slow cooling of 1 °C/min in order to minimize the formation of residual stresses. Annealing time was kept to be 1 h. The reduction was achieved in 10 passes during which initial thickness of plate (23 mm) was reduced to a final thickness of 8 mm. Such a series of thermomechanical processing (TMP) is known to give rise to a strong crystallographic texture with a majority of basal poles (or $<c>$ axis of the hexagonal unit cells) getting aligned towards the plate normal of the rolled samples [1]. Thus we have a set of binary alloys with well recrystallized microstructures and strong crystallographic texture. Such a set is ideally suited for studying deformation along different directions to bring out texture and composition dependent deformation behaviour. In addition, such a texture and microstructure being very common in the actual clad applications of Zr, the results of the present study are of immense practical use for the Zr industry.

Compression samples along three principal directions, *viz*, rolling, transverse and normal directions (RD, TD, and ND) have been extracted from the aforementioned TMP processed samples. These were cylindrical samples of 12 mm in length and 8 mm in diameter in case of deformation tests along RD and TD. Due to thickness limitation of the rolled samples (8 mm), sample dimensions for the tests along the ND were restricted to 8 mm in length and 6 mm in diameter.

The time of flight neutron diffraction beam line, ENGIN-X, at ISIS, Rutherford Appleton laboratory, UK, was used for the in-situ compression loading and diffraction experiments [21,22]. Diffraction spectra were acquired using two detectors (longitudinal and transverse), strategically positioned to capture the reflections from crystallographic planes lying parallel and perpendicular to loading direction of the samples. Such an arrangement allows the detection of "$\{10\bar{1}2\}\langle 10\bar{1}\bar{1}\rangle$" twinning in hcp materials (the most common mode of twinning in these materials [3,23]) since the change in orientation due to twinning results in appreciable changes in the intensity of certain reflections. Compression tests were performed along all RD, TD and ND. The compression tests were carried out in different control modes (regimes) during the in-situ experiments. Ideally, a constant strain rate would have been used throughout. However, to ensure enough data points were acquired and that the beam time was used efficiently, two control modes were used:

- Constant stress regime: The data points in the elastic regime (up to ~50 MPa below the macroscopic yield point) were captured in this mode. This ensured enough points were captured, which would not be possible if a constant strain rate had been used.
- Displacement controlled regime: Data points in the plastic regime (up to 0.18 true strain) were captured in this mode. In order to make effective use of beam time, the data points in the plastic regime were captured at two different strain rates: a slower rate of $7\times10^{-6}/s$until 0.025 strain followed by $2.8\times10^{-5}/s$ until 0.18 strain. The frequency of measurement points was increased around the yield point by the deliberate selection of lower strain rate.

It was found that an acquisition time of 5 mins gave an acceptable signal to noise ratio.

The microstructure of the materials was characterized using

SEM based Electron Back Scatter Diffraction (EBSD). EBSD samples were metallographically polished prior to electropolishing using a commercial system, Labopol. Electropolishing was done using 15 V and a temperature of 5 °C in an electrolyte of 80% Methanol+20% Perchloric acid. The EBSD measurements were carried out on a FEI Sirion FEG-SEM equipped with the HKL system. For the crystallographic texture measurement, low spatial resolution (step size of 50 μm) large area maps were recorded covering an area of 70 mm^2. A step size of 0.3 μm, covering 500 μm by 200 μm, was used for the more detailed scans of the microstructural details.

2.2. Model for prediction of twin evolution

Crystal plasticity finite element modelling (CPFEM) was used to simulate the deformation of the material with emphasis on capturing the observed twinning behaviour. A rate dependent three-dimensional CPFEM was employed for this purpose. Details of the original, two dimensional version of the same can be found in Ref. [24]. In this model, plastic deformation is assumed to occur by slip and twinning according to

$$\frac{\dot{\gamma}}{\gamma_0}=\left(\frac{\tau}{\tau_0}\right)^{\frac{1}{m}}, \quad (1)$$

where, $\dot{\gamma}$ is the slip/twin shear rate, γ_0 is nominal reference slip rate, τ is the resolved shear stress and τ_0 is the critical resolved shear stress (CRSS) for any given slip or twin system and m represents rate sensitivity. In this way, twinning was treated as directional pseudo-slip, the twinning shear rate being calculated identically to slip rate. As the deformation rates employed in the actual in-situ experiments of the present study are rather low, effects due to rate sensitivities are not expected to be significant. Hence, the model was also made rate insensitive by deliberately choosing a low m value of 0.02 for all slip/twin systems. Although it is arguable that twining is more rate insensitive compared to slip, under the conditions employed in the present simulations, application of even lower values of m for twining systems would not result in any noticeable changes in simulation predictions (of slip activity, plastic spin, local stress, and twinning evolution). This is owing to the fact very low value of m makes simulations results insensitive to minor local variations in strain rates.

In the simulations we used a constant low work hardening rate of $\Theta=100$ MPa for all slip/twin systems. Isotropic latent hardening was applied, i.e., the incremental change in CRSS for any slip/twin system is a function only of the sum of all slip shear increments, irrespective of the combination of active slip/twin systems. Only $\{10\bar{1}2\}\langle 10\bar{1}\,\bar{1}\rangle$ twin system was accounted in this model, in agreement with experimental observations of the present study (see next section). Twinning pseudo-slip (or shear due to twinning) occurs according to Eq. (1) on all six twin variants of a given integration point (IP). When the accumulated shear on the most active of the six twin variants (hereafter denoted by γ_{tw}) reaches a value γ_{lim}; the IP is instantaneously reoriented by 85° according to the geometry of the most active twin system. This way the model takes into account lattice reorientation due to twinning. After reorientation, a further ($\Gamma-\gamma_{tw}$) twinning shear is allowed on the originally most active twin system-based on the geometry before reorientation, again according to Eq. (1) ($\Gamma=0.17$ is the characteristic twinning shear for the $\{10\bar{1}2\}\langle 10\bar{1}\,\bar{1}\rangle$ twin in Zr). The limiting case of $\gamma_{tw}=\Gamma$ corresponds to a situation where the whole volume represented by the given IP has twinned. Due to the drastic hardening effect of twinning reorientation, it was found to be necessary to introduce disorder in the γ_{lim} values to achieve good fits to the experimental stress–strain curves. The γ_{lim} values were sampled from a homogeneous probability density function on the interval [0.0068, 0.119]. This procedure helped to smooth out the hardening contribution of twinning. This randomness is expected to account for innumerable uncertainties of real situation (such as localized dislocation structure, its distribution etc). Earlier work has shown that good results can be achieved by treating all these factors as random fluctuations in the critical stress required for nucleating a twin [25]. The present model, on the other hand, introduces randomness in the reorientation part of the twinning process, but not in the CRSS of the twinning. This makes twinning to be strictly governed by the stress state and actual occurrence of reorientation of the twin volume to be subject to random fluctuation in shear strain from the instance of nucleation of twin. This approach has the effect of smoothening the stress–strain curves making them closer to experimentally observed ones, without affecting the twinning probability, which by design was made to depend solely on the value of CRSS.

The simulated system consisted of $15\times15\times15$ twenty-node iso-parametric brick elements, each containing 8 integration points (IPs). One element corresponded to one grain, i.e., all IPs of an element were assigned the same orientation. The orientations were randomly sampled from experimental EBSD based texture data and the resulting texture was cross checked to represent the experimental texture. Uni-axial compression simulations were performed by assigning the applied uni-axial compression strain tensor increment at every time step to all boundary IPs on the two opposing faces perpendicular to the loading direction. In general, the residual stresses present in the samples can have significant bearing on the observed flow response of the materials [26,27]. However, in case of present study, owing to the similarity in the processing conditions, the extent and distribution of the residual stresses are expected to be rather similar among all of the samples at the beginning of the in-situ deformation. The role of residual stresses, if any, was accounted indirectly by appropriate values of CRSS of the different slip systems in the present model.

3. Results

The initial microstructure and crystallographic texture of the samples used in the in-situ deformation studies are shown in Fig. 1. For the purpose of brevity, only results of the lowest (Fig. 1a) and highest Sn (Fig. 1b) alloys are included here. It is evident that samples were fully recrystallized with characteristic crystallographic texture. Further, both samples were similar in their microstructure and texture distribution (as represented by the respective IPF plots and pole figures). It is important to note that microstructures and textures of other two intermediate compositions (0.23% and 0.33% Sn) were indeed similar to the ones presented in Fig. 1. As can be seen in Fig. 1, the starting texture has the basal poles aligned towards ND of the sample, with a $\sim\pm30°$ spread along TD. There was also a preferred alignment of the $11\bar{2}0$ poles towards RD. The average grain size of these initial un-deformed samples was found to be 5.5 μm for Zr–0.15%Sn, 4.5 μm for Zr–0.23%Sn and 5 μm for Zr–0.33%Sn and 4.5 μm for Zr–1.2%Sn. Thus the four materials are comparable in their initial microstructure, texture, and grain size distribution. Thus the systematic variation of the measured properties must be associated with the differences in Sn content and loading direction only.

3.1. Flow behaviour as a function of composition and deformation direction

The flow behaviour of the Zr–Sn alloy samples is depicted in Fig. 2 as a function of Sn content and deformation direction. These curves are from the data collected during in-situ diffraction experiments. The following key observations can be made from the figure:

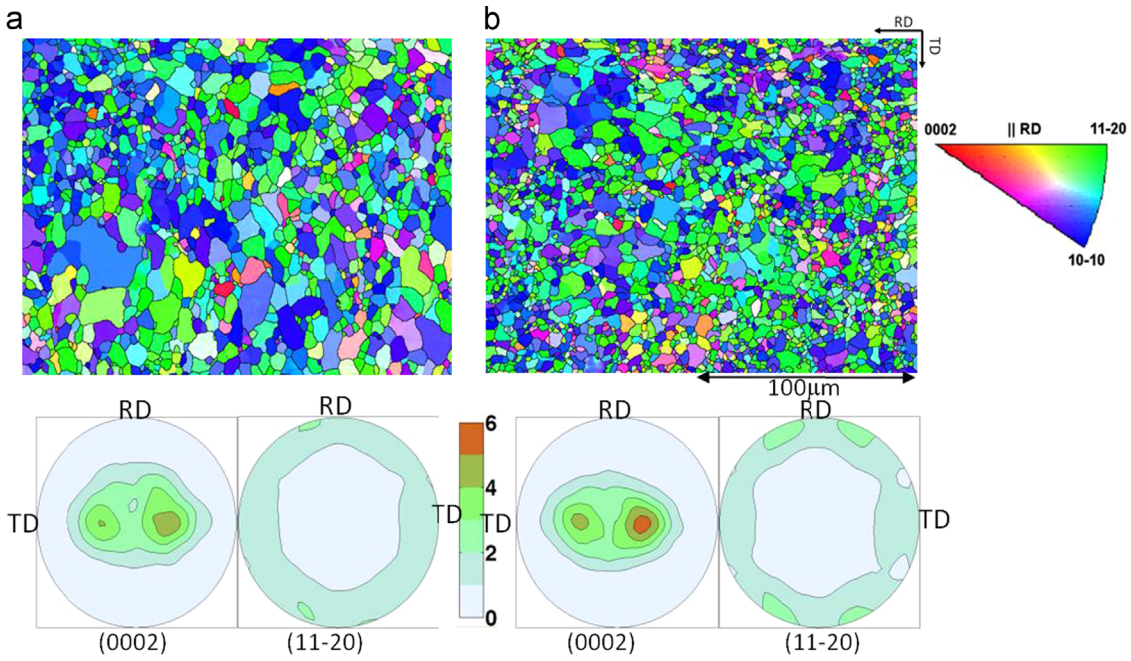

Fig. 1. Initial microstructures (before in-situ deformation/diffraction studies) (a) Zr–0.15%Sn and (b) Zr–1.2%Sn along with respective pole figures of (0002) and (11$\bar{2}$0) poles. Maps are IPF colour coded. Similar colour coding has been used throughout the manuscript for the depiction of IPF colour coded EBSD maps and the pole figures.

1. There is a systematic increase in the flow stress with increase in Sn content for all directions (RD, TD and ND). This confirms the expected solid solution strengthening effect of Sn. As expected, the increase in flow stress was found to be non linear with respect to Sn content. The flow data is summarized in Table 2, showing that the relative increase in the yield stress ($\Delta\sigma_y$) is higher at lower Sn values, as if the strengthening effect of Sn saturates at high Sn content. This was the reason for choosing three alloys with a comparatively small difference at the low scale of Sn content and only one with a significantly higher value.
2. The flow stress for a given Sn content, increases in the order of deformation along RD, TD and ND, signifying strong effect of texture on the deformation, see Fig. 2 and Table 2.
3. Along RD, the flow curves, exhibit comparatively low strain hardening regime (referred hereafter as the 'flat response') during the initial stage of plastic deformation. This flat response is increasingly pronounced with increasing Sn content, see Fig. 2a. A magnified plot of this regime is included in the figure to bring out this effect more clearly.
4. There is a conspicuous absence of such a flat response regime in case of compression tests along ND. The behaviour of TD samples is closer to that of ND samples as no distinct 'flat response regime' was observed.
5. Along RD the strain hardening also increases with Sn content. This is not seen along TD or ND.

In summary, the role of Sn on the flow behaviour was seen to be highly dependent on deformation direction, that is, it is strongly affected by the texture.

3.2. Evolution of intergranular elastic strains (diffraction elastic strains) as a function of composition and deformation direction

The evolution of the intergranular elastic strains for three principal families of grains: 0002, $10\bar{1}0$ and $10\bar{1}1$ is shown in Fig. 3. The data represents the relative change in the elastic strains from the initial (before loaded) state and corresponds to compressive strain along the loading direction. As expected, all the curves show an initial linear response corresponding to elastic deformation at low stress levels. The onset of plasticity is marked by a deviation from linearity and is a function of Sn content. An observation of particular interest is the behaviour of 0002 reflection. As can be seen, for loading along RD and TD deformations, the elastic strain first increases at a constant applied stress, and then relaxes significantly. This is a clear signature of tensile twinning (i.e., $\{10\bar{1}2\}\langle 10\bar{1}\,\bar{1}\rangle$). On the other hand, for samples loaded along ND, one can infer that there was no $\{10\bar{1}2\}\langle 10\bar{1}\,\bar{1}\rangle$ type of twinning.

The decrease in the elastic strains by the grain families $10\bar{1}0$ and $10\bar{1}1$ indicate the occurrence of plastic deformation. This "unloading" was more pronounced at higher Sn contents.

3.3. Onset and evolution of twinning

In Zr and most other hcp metals, the most common twinning mode is the $\{10\bar{1}2\}\langle 10\bar{1}\,\bar{1}\rangle$ twin. This twin induces a tensile strain along the $<c>$ axis and is therefore particularly active during compression of rolled and recrystallized material along RD and TD. Under the measurement conditions used, the formation and evolution of these twins causes appreciable changes in the intensity of the 0002 reflection, decreasing in the transverse and increasing in the longitudinal detector. This is because of the 85° lattice rotation caused by twinning. Therefore, the integrated intensity of the 0002 reflection can be used to determine the critical macroscopic stress and strains needed for the onset of twinning and monitor evolution of twinning during deformation. The data collected by the longitudinal detector (i.e., along deformation direction) is shown in Fig. 4. Following inferences can be drawn from the figure:

1. The extent of twinning (as measured by change in integrated intensity) is highest for loading along RD, followed by loading along TD. Deformation involving compressive loading along ND, however, did not result in the formation of any detectable change in 0002 intensity, indicating absence of "{1012} $<1011>$" twinning.

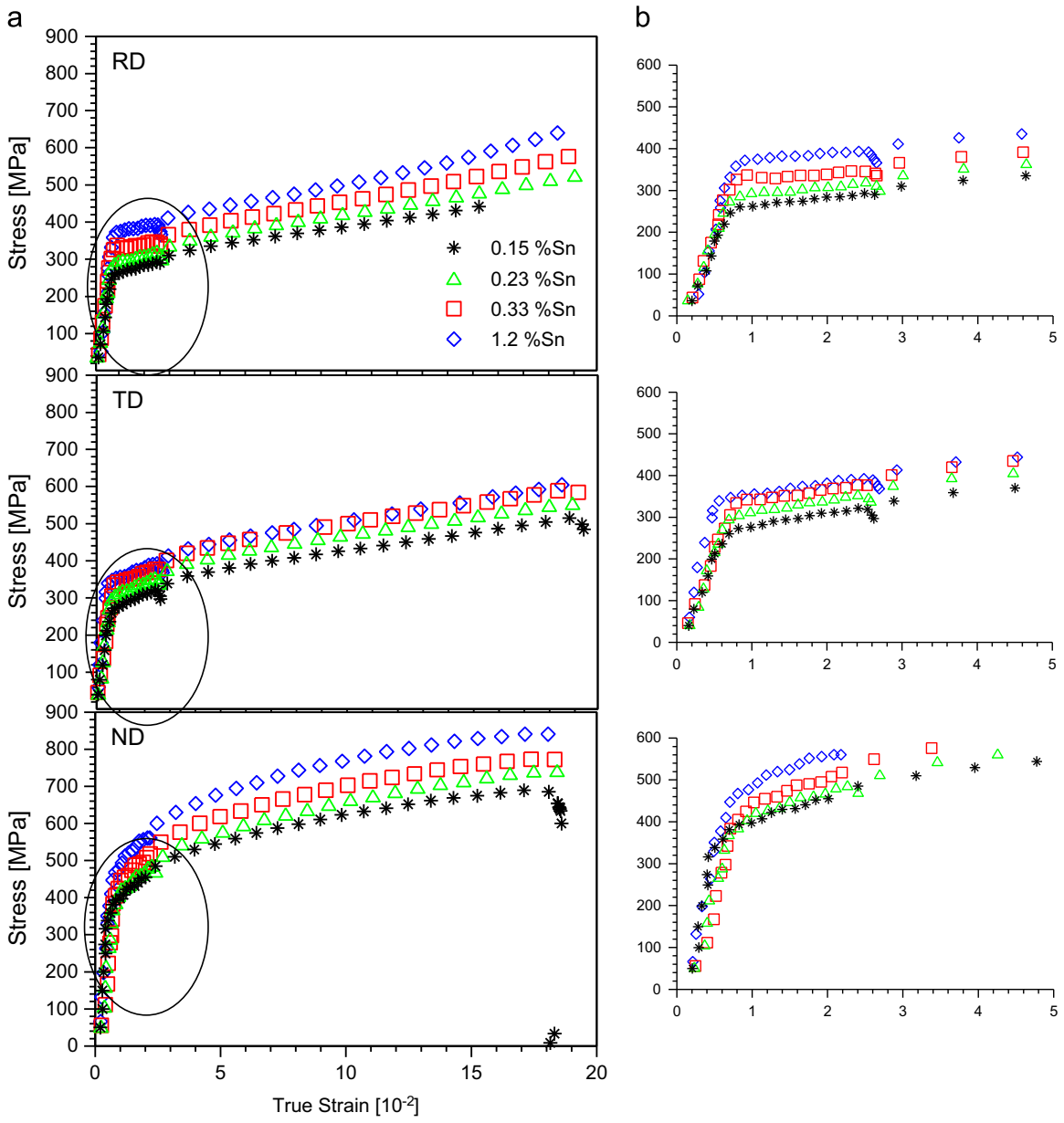

Fig. 2. (a) Flow curves of the Zr–Sn alloys subjected to compression experiments along three different directions, i.e., RD, TD, and ND. (b) Zoomed in version of the circled parts of (a), i.e., low plastic strain regime.

Table 2
Macroscopic yield points for Zr–Sn alloys as determined in the present study.

Alloy	Yield stress (MPa)		
	RD	TD	ND
0.15% Sn	260	270	400
0.23% Sn	281	300	420
0.33% Sn	303	350	450
1.20% Sn	352	360	500

2. In the RD case, there is a clear and strong effect of Sn content. Higher Sn content corresponded to higher extent of twinning. In contrast, the extent of twinning for TD deformation appears to be very weakly dependent on Sn content. While the lowest Sn content alloy shows an increase of 0002 intensity by 15 times (nominal values), for a strain of 0.15 along RD, the sample with 1.2%Sn shows an increase of as much as 32 times for the same extent of deformation. In the TD case, however, the change in 0002 intensity increases only marginally with Sn content (Fig. 4). This suggests a weak dependence of the extent of twinning on the Sn content for deformation along TD. It may be emphasized here that although the extent of twinning in TD is lower than in RD, it was nevertheless quite appreciable, unlike during loading along ND.
3. The critical strain needed for the onset of twinning in both RD and TD deformations is fairly independent of the Sn content. On the other hand, critical stress required increases with Sn content in both RD and TD cases.

The in-situ diffraction data can also be used to extract intergranular strains of the parent grains, which twin during deformation, as shown in Fig. 5. Diffraction elastic strains were calculated from the peak shifts of the 0002 reflection using transverse detector. For the sake of clarity, only the results of two extreme compositions for RD and TD deformations are included in

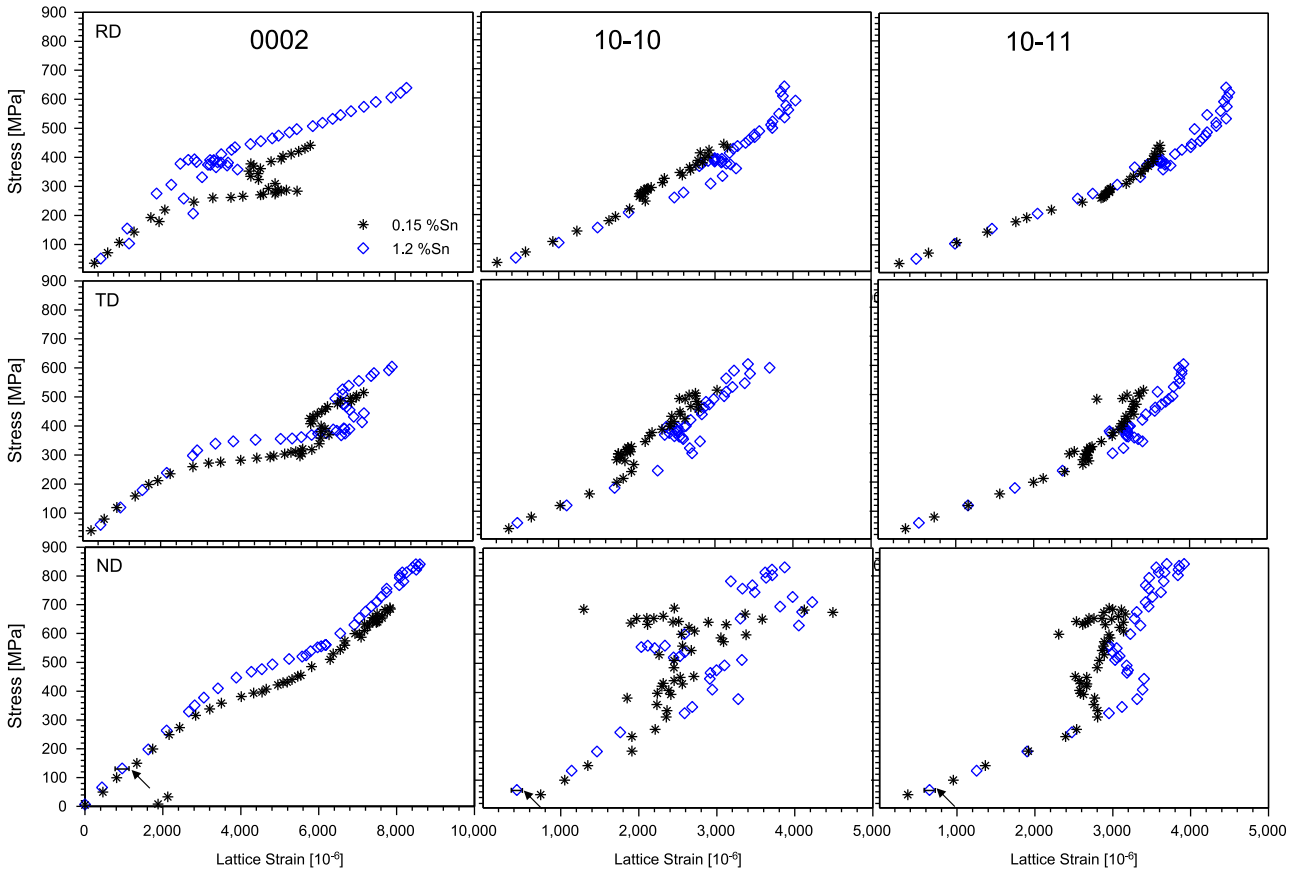

Fig. 3. Evolution of compressive intergranular strains (diffraction elastic strains) of grain families corresponding to 0002, $10\bar{1}0$ and $10\bar{1}1$ reflections for Zr–0.15%Sn and Zr–1.2%Sn during compressive loading along RD, TD and ND. For the purpose of clarity, only two alloys (representing extremes of composition) are shown in the figure. The behaviour of the excluded alloys lied in between these two alloys. The data is computed from the peak shift of the respective reflections as recorded by the longitudinal detector. Thus the strains correspond to those along the loading direction of the sample. The measurement uncertainty in lattice strain measurement was ± 50 με under the measurement conditions used [20] and the same is indicated in the form of error bars on selected points (pointed out by the black arrows in the ND plots). Note that the stress and strains in the figure are compressive in nature and negative sign was omitted.

the plots. The onset of twinning is marked on the plots using arrows. The samples were oriented in such a way that in both, the RD and TD deformations, the transverse detector measured lattice strains along samples' ND (plate normal). As can be seen, the relative difference in the intergranular strains of the twinning grains of alloys with different Sn contents is similar for both RD and TD deformations.

Direct and conclusive evidence for the twin formation and determinations of the type of twins was obtained with microstructural characterization of the deformed microstructures using EBSD. Fig. 6 shows the microstructure of the four compositions used in the present study after 18% compression along RD[1]. These maps show that twins are indeed of "$\{10\bar{1}2\}\langle 10\bar{1}\,\bar{1}\rangle$" type, as expected. Further, these microstructures are in full agreement with the in-situ loading and diffraction results presented in Fig. 4, in terms of twin volume fraction. These maps confirm that volume fraction of twins increases with Sn content, for RD loading. Another important observation from these micrographs is that the increase in volume fraction of twins for higher Sn contents is due to larger number of twins rather than due to bigger twins.

The effect of loading direction is illustrated in Fig. 7, where the TD and ND deformed microstructures of the highest Sn alloy are shown. These microstructures also confirm that the twinning propensity is indeed less for loading along TD and negligible in ND deformations. In addition, no other modes of twinning other than $\{10\bar{1}2\}\langle 10\bar{1}\,\bar{1}\rangle$ type were observed in these samples.

The significant difference in the role of Sn, on the twining behaviour, in case of compression along RD and TD was further corroborated by the deformation textures. Fig. 8, illustrates the basal pole figures of the deformed samples of the two extreme compositions subjected to compression tests along the RD and TD. Comparison of these pole figures with ones shown in Fig. 1 reveals that there is considerable increase in pole intensities along the RD axis of the pole figure in case of samples compressed along RD. This is essentially due to activation of $\{10\bar{1}2\}\langle 10\bar{1}\,\bar{1}\rangle$ twins. The extent of difference in the twining between samples with different Sn contents is noticeable through difference in the intensity levels of the texture component along RD axis (highlighted by the circles). It is clear that higher Sn sample had higher intensity of this texture component. Compression along TD on the other hand resulted in the insignificant differences in the distribution of basal pole intensities in the samples with different Sn contents. These observations are thus in direct agreement with the neutron diffraction based twin evolution interpretations.

4. Discussion

There are three main discussion points. Firstly, the RD samples showed an anomalous flat response regime, the extent of which

[1] The sample with 0.15%Sn had only 0.15 strain as the in-situ neutron diffraction and deformation test had to be interrupted at this strain due to unexpected issue in the machine. Nevertheless, the amount of deformation is close enough to other samples (which had 0.18 strain) to make '*qualitative*' comparison of the corresponding microstructures for the extent of twining.

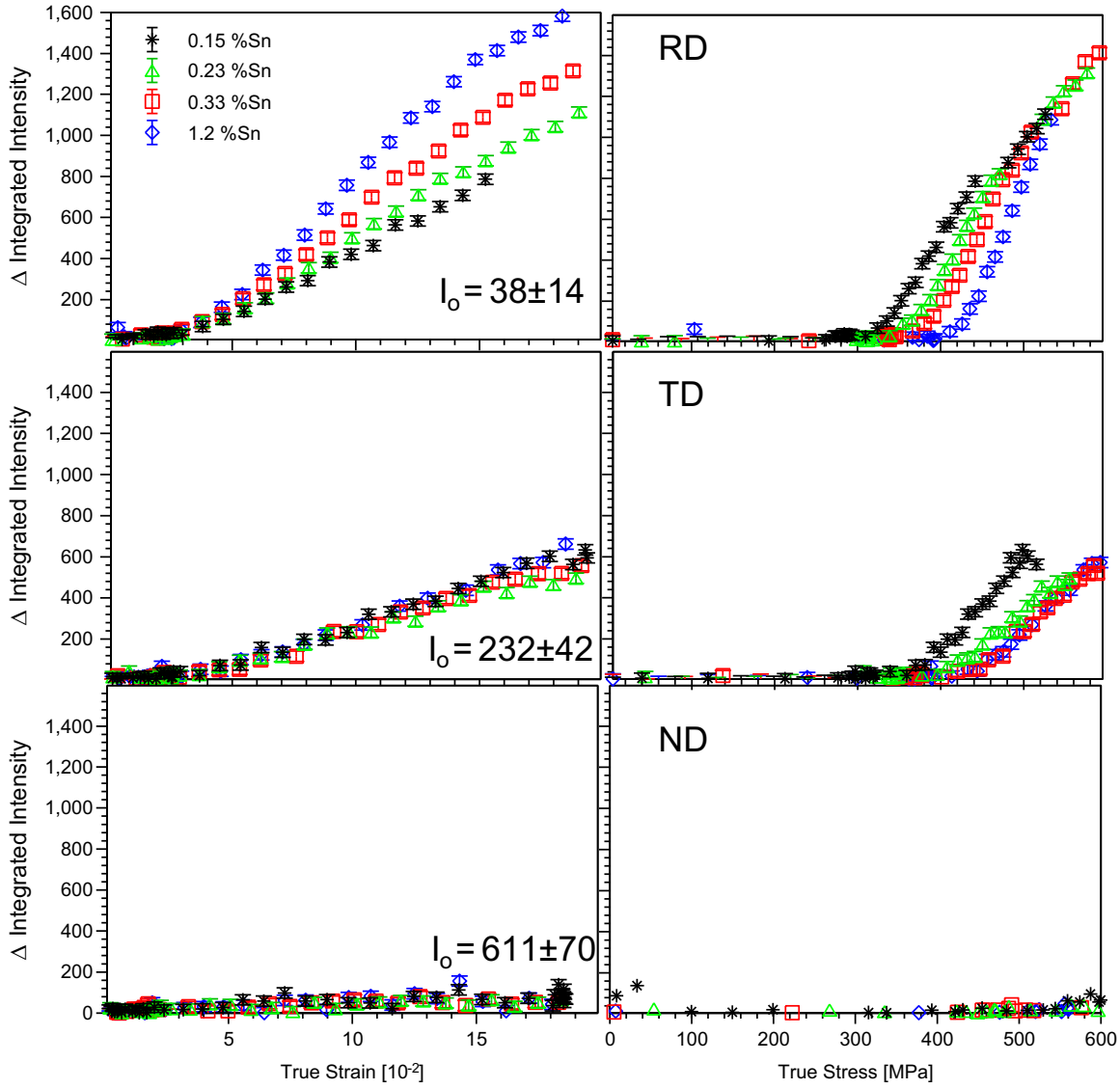

Fig. 4. Change in integrated intensity of (0002) reflection for all four alloys as a function of applied (a) strain and (b) stress. I_o values included in the plots represent the mean initial intensify of the unloaded (initial state) samples.

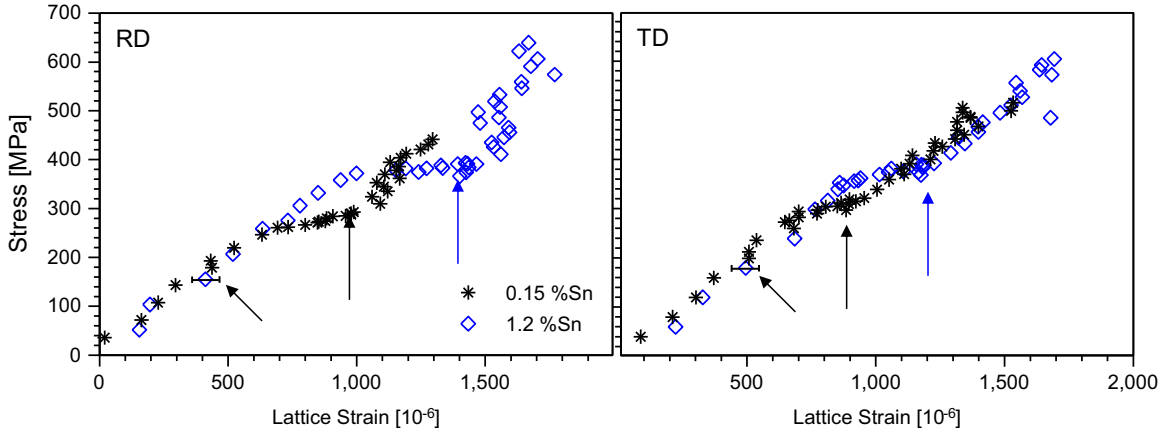

Fig. 5. Intergranular lattice strain evolution of 0002 family of grains recorded from transverse detector. The inflections in the curves represent the onset of twining (indicated by vertical arrows) and thus the strain state and corresponding stress state at the time of twin nucleation of the parent grains of twins. The measurement uncertainty in the lattice strain is indicated by the error bars (pointed by the inclined arrows) for selected points of the two plots.

increased with increasing Sn content. Secondly, while the extent of twinning strongly depended on Sn content in the RD case, it is only weakly dependent on Sn content in the TD case. Finally, whereas the critical macroscopic strain at the onset of twinning was independent of Sn content and loading direction (RD and TD), the stress level at the onset of twinning increased noticeably with

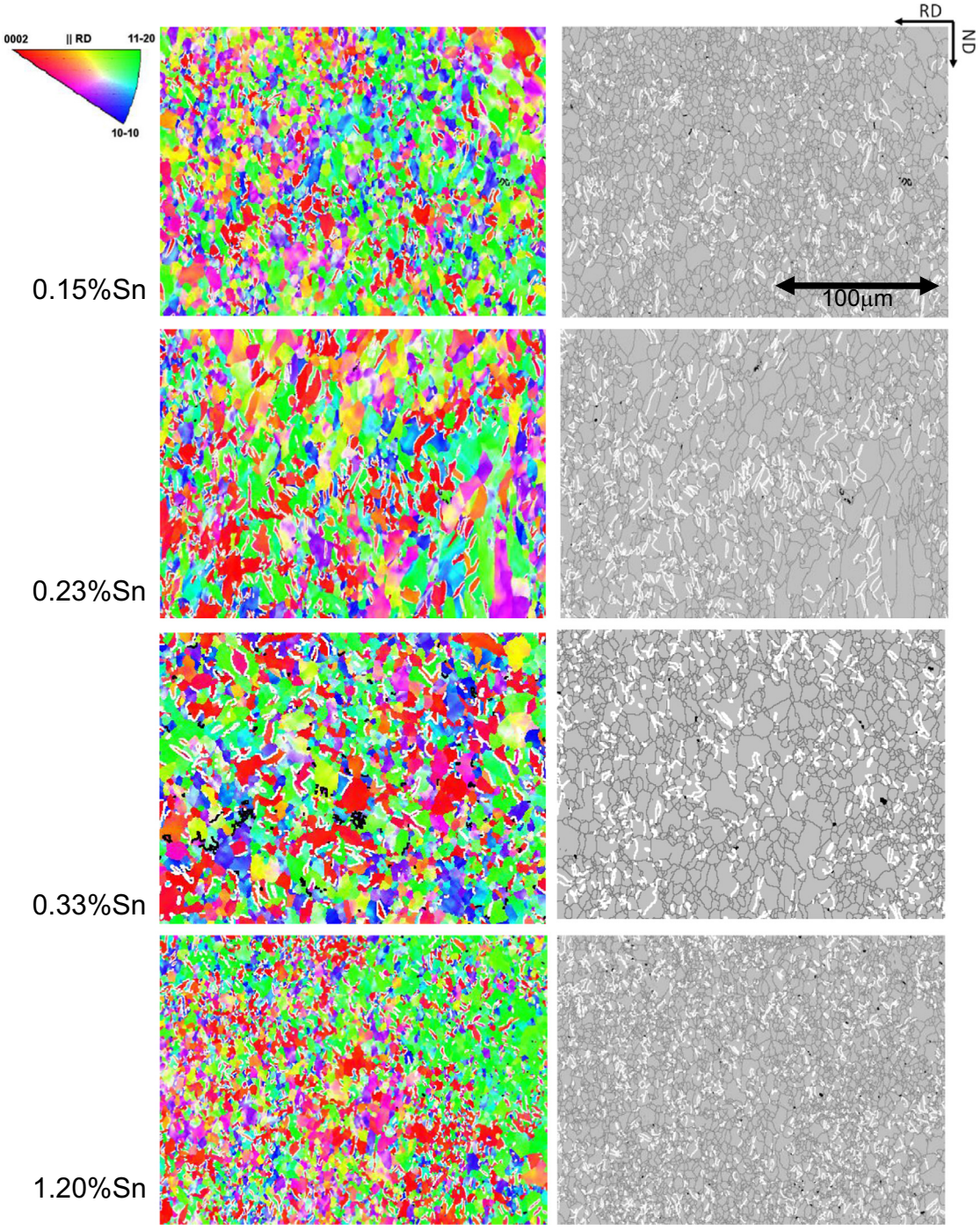

Fig. 6. IPF colour coded EBSD maps showing the twinning behaviour as a function of Sn content for RD deformed samples. These microstructures were recorded from samples subjected to a compressive strain of 18%. The grey scale maps show the twin boundaries (with misorientation corresponding to 85° tensile twins) demarcated with white lines for better visualization of twins.

Sn content, independently of loading direction.

4.1. Role of Sn on slip systems

The anomalous flat response in the stress–strain behaviour of the alloys was earlier attributed to the presence of thermal residual stresses in the material, caused by large differences in the thermal expansion coefficients along the $<a>$ and $<c>$ axis of the hcp unit cell [28,29]. In this study, the extent of this flat response was seen to increase with Sn content. The potential reason for this effect could be as follows. The initial texture of the samples compressed along RD was such that a majority of the grains had favourable orientation for the prismatic slip, i.e., $<a>$ type slip on prismatic planes. It has been shown previously that in case of prismatic slip, interaction among dislocations of different prismatic planes in general is low resulting in low strain hardening [30], which correlates well with the flat regime observed. In addition, modelling work has shown that the $<a>$ type dislocations in α-Zr undergo dissociation into partials creating stacking faults, which are stable in the prismatic plane, since the stacking fault energy in the basal plane is too high [12,31]. The addition of Sn to Zr is known to dramatically decrease the stacking fault energy of the system as shown in. Fig. 9, from Ref. [32]. This drop is more prominent at low Sn additions and saturates at high Sn

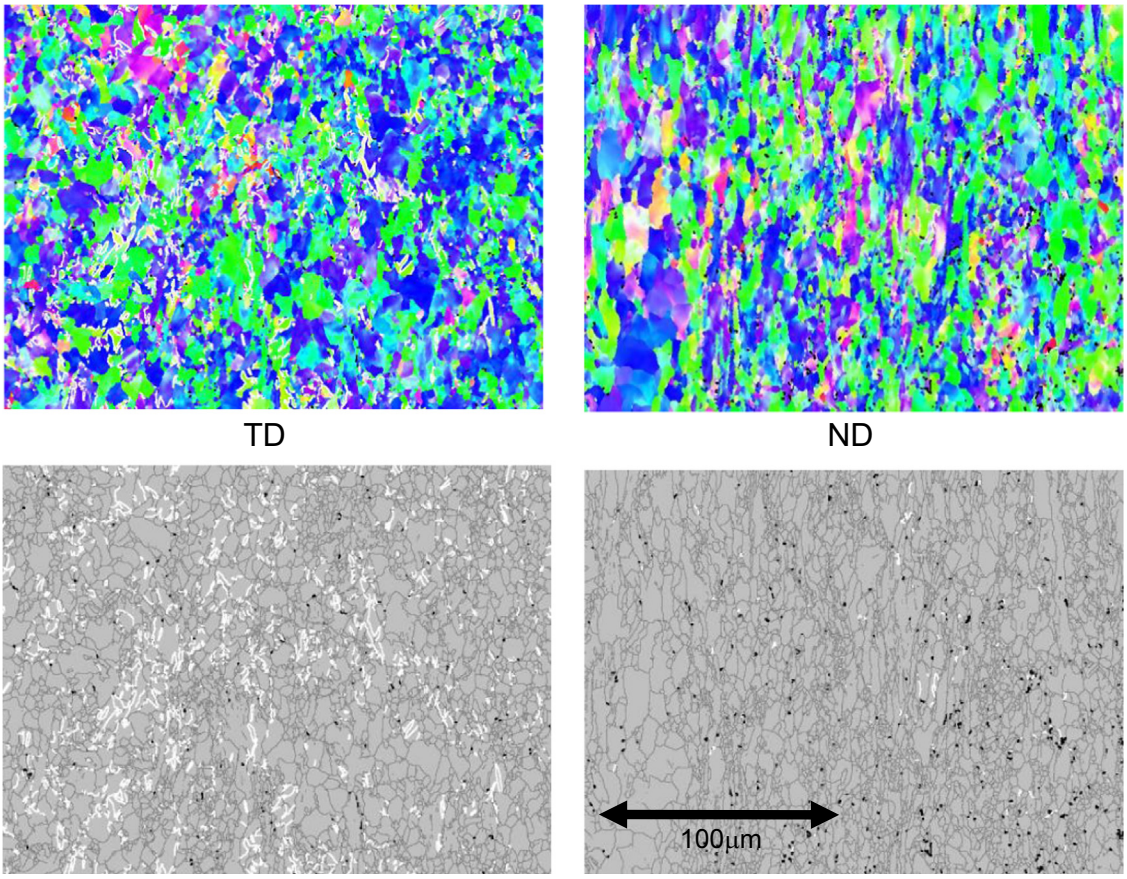

Fig. 7. EBSD maps showing the twinning behaviour as a function of deformation direction for alloy with 1.2%Sn at 18% compressive strain. Compare these microstructures with the last one of Fig. 6. These maps confirm that only TT1 twins form even in TD and no significant twins are seen in ND deformation.

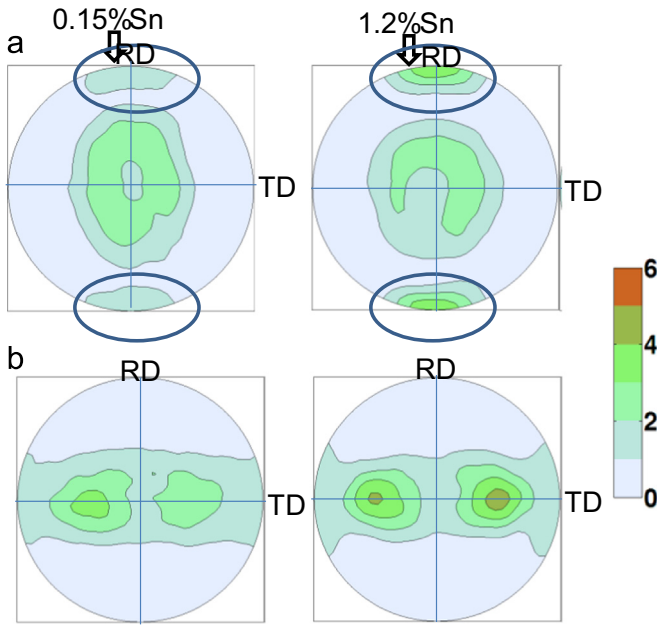

Fig. 8. Basal pole (0002) figures of deformed microstructures representing the deformation textures (a) compression along RD (b) compression along TD. The directions RD and TD shown on the pole figures represent sample coordinate system. The ellipses highlight the texture components that arise due to twining activity in case of compression along RD.

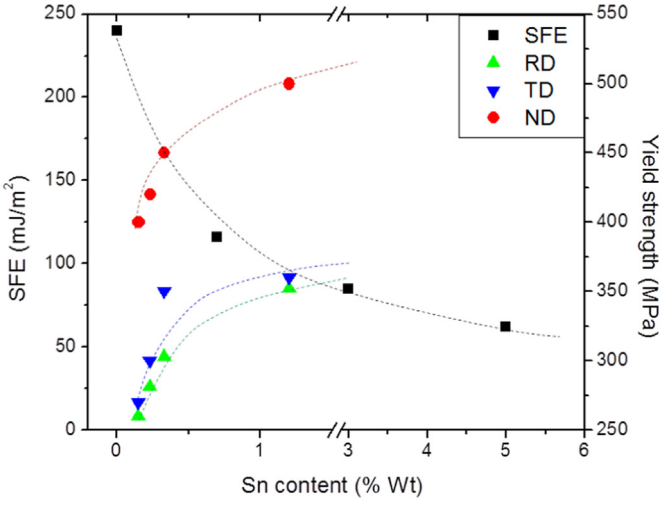

Fig. 9. Variation of stacking fault energy (SFE) as a function of Sn content of the alloy [29]. For easy comparison, the macroscopic yield stress values corresponding to different compression directions (RD, TD and ND) are also shown on second *Y* axis (on the right). It is evident that non linearity of role of Sn content on the mechanical properties follows similar trend as that of the SFE Vs Sn content. (Please note the break in *X* axis).

contents. This correlates with the observed non-linear effect of Sn on the flow stress, discussed in Section 3. In addition, the yield point data presented Fig. 9 is consistent with the classical understanding of many solution strengthening models which predict square root dependence of yield point on the concentration of the solute atoms. The drop in SFE should, in principle, increase the stacking fault width and thus promote planar slip. Thus, increasing the Sn content not only makes the initial barrier for dislocation motion higher, but is also likely to increase the planarity of slip, which could decrease the potential strain hardening,

leading to the observed pronounced flat response regime in RD compression. The absence of a marked flat response in ND compression further corroborates this argument. In this case, very few grains are in favourable orientation for the activation of $<a>$ type and therefore no flat regime is observed [33]. In this case, however, since very few grains are in favourable orientation for the activation the $<a>$ type slip, $<c+a>$ slip can be one of the principal modes of deformation. The observed increase in yield stress with Sn content, in this case, signifies that the CRSS of slip by the $<c+a>$ mode is also influenced by the Sn content.

4.2. Twinning behaviour

The lack of an effect of Sn content on the extent of twinning in TD loading, in stark contrast to the strong effect observed in RD loading, is rather intriguing. Before delving further into possible explanations, it is important to clarify that this observation is not due to a failure of capturing subtle changes on account of poorer statistics due to the lower twin volume fractions in the TD case. As pointed out in Section 3.3 (point 2), the extent of twinning is lower but still considerable in TD deformation.

The assertion that Sn did not affect the extent of twinning in TD compression was also supported by the flow behaviour of the material. As can be seen in Fig. 2, the strain hardening is higher at higher Sn contents along RD, which can be attributed to twinning. The flow curves for TD compression do not show any difference in the strain hardening. This signifies that the extent of twinning was rather similar in all alloys for compression along TD. This implies that the effect of Sn content in twinning depended on the loading direction.

As far as extent of twinning is concerned, present results show that RD compression had the highest, followed by TD and virtually absent in case of ND compression. The fact that the $\{10\bar{1}2\}\langle 10\bar{1}\,\bar{1}\rangle$ requires tensile stress along $<c>$ axis can explain this observation, as the initial texture of the material (see Fig. 1) renders such stress state to exist more in case of RD than in TD (and ND) for a majority of grains. However, this explanation does not 'seem' to be sufficient to explain the apparent strong effect of Sn on extent of twinning for compression along RD but complete lack of it for compression along TD. To probe if the alloys with different Sn contents in RD and TD compression, had any other differences that might help explain the observed behaviour, the evolution of the diffraction peak broadening, a finger print of plastic activity, was analysed. However, even this could not delineate RD compression from TD compression as both have similar signatures of peak broadening evolutions. Since the FWHM and intergranular strain analysis could not explain the dependence of loading direction on the effect of Sn content on twinning, crystal plasticity finite element modelling (CPFEM) was employed to test simple twinning criteria for the two different loading conditions. For the purpose of brevity, only the two extreme compositions were considered for the simulations. Initially, several simulations were run with varying CRSS values for the slip/twin systems to reproduce the observed flow behaviour.

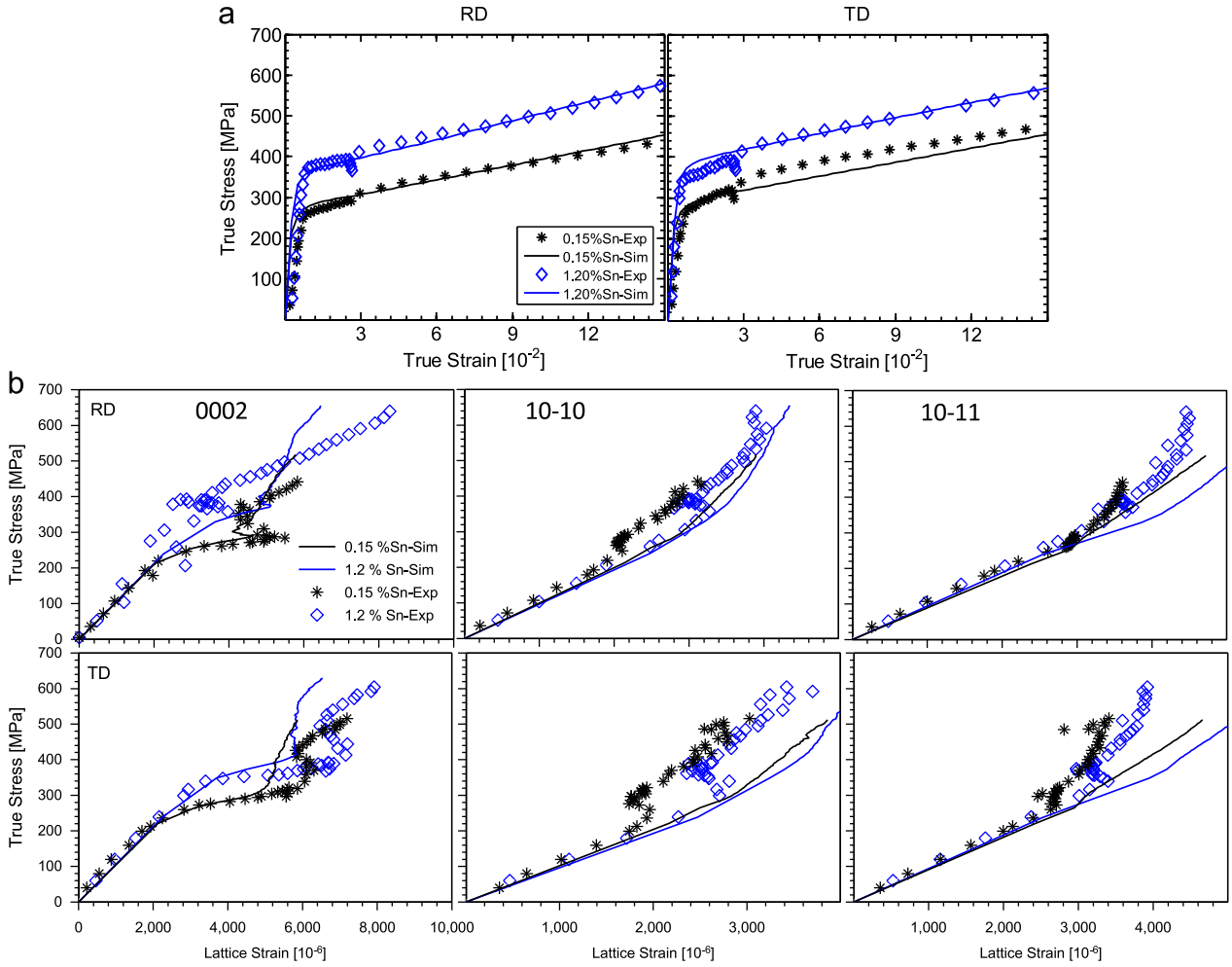

Fig. 10. Comparison of CPFEM simulations with experimental (a) flow curves (b) Intergranular lattice strains for various grain families for respective compression tests along RD and TD.

Table 3
CRSS values (in MPa) for various slip/twin systems used for present simulations.

Slip/twin system	0.15%Sn	1.2%Sn
$\{0001\}\langle\bar{1}2\bar{1}0\rangle$ Basal slip	110	160
$\{10\bar{1}0\}\langle\bar{1}2\bar{1}0\rangle$ Prismatic slip	90	125
$\{10\bar{1}1\}\langle\bar{1}\bar{1}23\rangle$ Pyramidal slip	360	400
$\{10\bar{1}2\}\langle10\bar{1}\bar{1}\rangle$ Tensile twin	200	200

Fig. 10 represents the best fit simulations in which excellent agreement between experimental and simulated flow curves (Fig. 10a) and intergranular strains for important grain families (Fig. 10b) can be seen. Table 3 gives the CRSS used for these simulations. It may be noted that while CRSS values for slip was assumed to change with Sn content, the CRSS values for twinning was not. In fact, this difference in how Sn affects slip and twinning is responsible for the difference in twinning activity with Sn content for RD compression. It is clear that the model, apart from capturing the flow curves very well, could also simulate the observed evolution of intergranular lattice strain evolutions fairly well, particularly the behaviour of 0002 family of grains. This family is of particular interest to the present study as this is the reflection which is most sensitive to twining behaviour of the samples. As can be seen, the difference in the observed stress level for twin initiation between the samples of different Sn contents (in spite of using same twining CRSS for both high and low Sn alloys) was well reproduced. In addition, the abrupt elastic unloading of the intergranular strain (of 0002 reflection) subsequent to twining is captured well by the model. This is a significant improvement over the previous works in which sudden relaxation due to twining could not be simulated [4].

The extent of twinning predicted by simulation is compared with experimental observations in Fig. 11. Since the extent of twinning from experiments is known only in terms of change in integrated intensity (in arbitrary units), a direct comparison with the volume fraction estimations from simulation is not possible. For a meaningful comparison, we need to consider the experimental integrated intensity and the simulated volume fraction relative to the initial integrated intensity in the experiments and the initial volume fraction in the simulations respectively, for both RD and TD. The respective experimental and simulated data is plotted using two y-axes in Fig. 11 for both RD and TD as a function of applied strain (Fig. 11a) and applied stress (Fig. 11b). To achieve a meaningful comparison, as mentioned above, the ratio of the y-axis limits was chosen to be the following: $R=E_0/S_0 \cdot f$, where E_0 is the initial experimental intensity, S_0 the initial volume fraction in the simulations and f is a correction factor. $E_0=40.8$, $S_0=0.00295$ for RD and $E_0=197.9$, $S_0=0.01085$ for TD. $f=0.62$ for both RD and TD compressions. The fact that f is fairly close to unity and independent of loading direction shows the quality and consistency of the model in terms of predicting the orientation changes due to twinning. It may be noted that the twin volume fractions from the simulations were calculated by considering the change in the integration points (IPs) with their c-axis within $\pm 15^\circ$ of the loading direction, which corresponds to the acceptance angle of the neutron diffraction detectors..To account for both the twinned and non-twinned (parent) orientations of an IP, the following weights were used in the calculations: $w_{tw}=\gamma_{tw}/\Gamma$ for the twinned orientation and $w_{pa}=(1-\gamma_{tw})/\Gamma$ for the parent orientation. w_{tw} and w_{pa} represent the volume fraction of twin and parent for the given IP. There is excellent agreement between the model predictions of twinning extent with the experiments for both RD and TD as

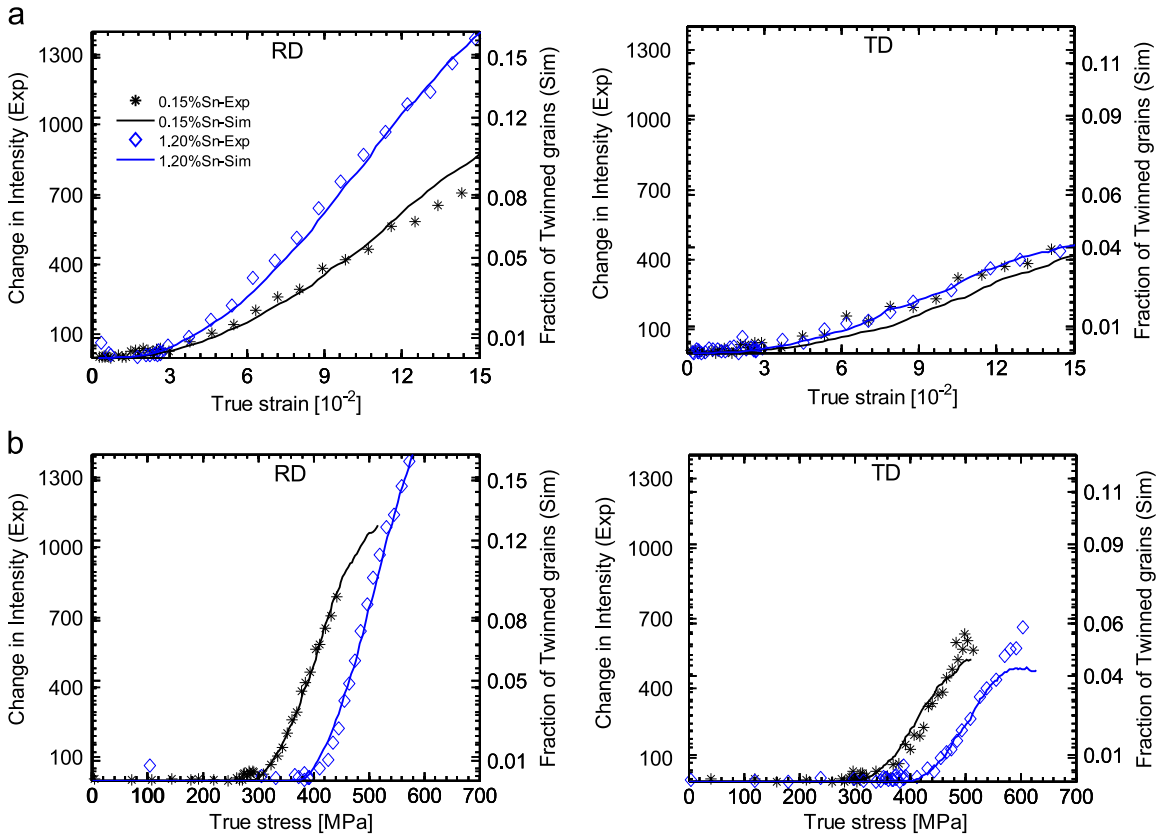

Fig. 11. Comparison of experimentally measured change in the 0002 integrated intensity (a measure of twinning extent) along with the CPFEM simulated weighted fraction of grains with their c-axis within 15 ° of deviation from the loading direction (i.e., fraction of twinned grains) for RD and TD deformations of two extreme compositions a function of (a) applied strain (b) as a function of applied stress.

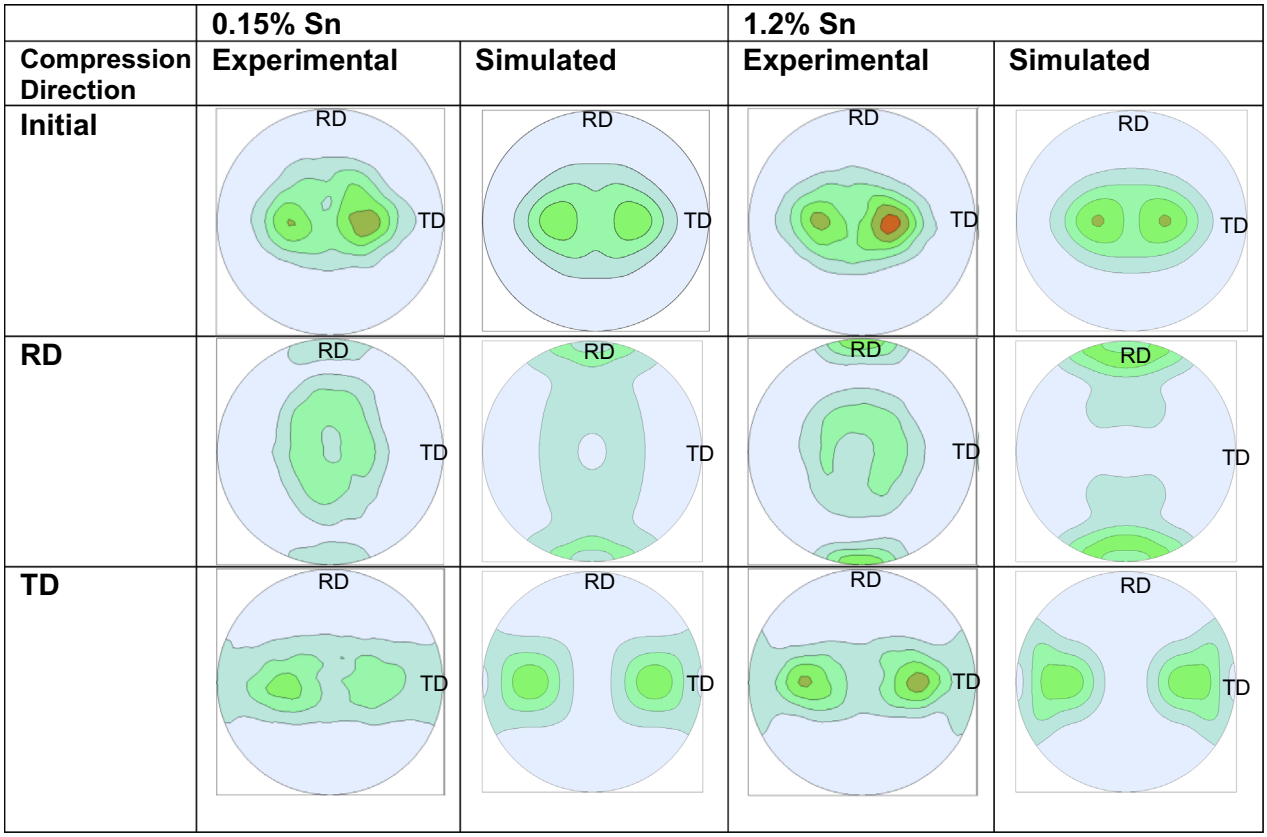

Fig. 12. Comparison of experimental and simulated textures of two alloys with extreme Sn contends (considered in the present study) for the case of two compression directions (RD and TD).

revealed by Fig. 11. The agreement between the simulations and experiments can also be independently seen through the comparison of corresponding textures. Fig. 12 depicts this aspect, where in the similarity in the predicted textures with that of the experimentally determined ones is evident. The slight differences between them can be attributed to the symmetrisation of the initial textures for the simulated textures. This was done to avoid artificial biasing that can arise due to either under or oversampling of certain orientations. The simulations, predict that the extent of twinning is directly proportional to Sn content for RD compression but insensitive for compression along TD, in full agreement with the experiments.

In the model Sn only affects the deformation by changing the CRSS for slip. In other words, the increased extent of twinning in RD for the high Sn alloy is a direct consequence of the higher flow stress and ultimately higher intergranular strains once plastic deformation starts. It should be noted that twinning only starts after some level of slip, i.e. when the intergranular strains, generated during deformation, result in stresses in grains orientated for twinning that exceed the twinning CRSS value. Without slip this is not possible regardless of the Sn content. The fact that such an increase in twinning extent was not seen in the TD simulations (despite using the same higher CRSS values for the higher Sn alloy) establishes that the starting texture is crucially important as it affects the intergranular strains/stresses evolving during the early stage of plasticity. The present CPFE model, assuming a CRSS criterion for twinning, demonstrates that compression along a direction that predominantly activates prismatic slip (*c*-axis predominantly perpendicular to the loading axis) generates intergranular strains that will more easily activate twinning than a compression direction with a greater mixture of prismatic and basal slip activity (*c*-axis is predominantly 60° off the loading axis). The model highlights that simple stress considerations can, at least in the present case, explain significant variations in twin activities of the samples with different starting textures.

5. Conclusions

The present investigation aimed at identifying the relative role of starting texture, stress and plastic strain on the deformation twinning behaviour of a binary Zr-alloy by varying alloy composition and crystallographic texture in a controlled manner. The major conclusions drawn from the study are as follows:

- Zr–Sn binary alloys with a characteristic split basal texture exhibit the highest extent of deformation twinning (tensile twins) when deformed along the original RD, followed by relatively low level of twinning in TD deformation. In case of ND no deformation twinning was observed.
- Analysis of the flow behaviour as a function of deformation direction (or texture) showed that $< a >$ type slip significantly affected by Sn. The initial zero hardening behaviour when compressing along RD, which becomes more pronounced with increasing Sn content suggests that Sn enhances prismatic slip planarity.
- For RD compression, increasing the Sn content results in a higher extent of twinning. In TD deformation, however, there is no difference in the extent of twinning in alloys with different Sn contents.
- A CPFE model that accounts for the multiple slip modes in Zr and incorporates twinning based on a critical resolved shear stress criterion reproduced successfully all of the experimental observations of twin evolution (in terms of twin volume

fractions and intergranular strain evolutions). The model demonstrates the importance of the starting texture when comparing twin activities and suggests that the intergranular strains generated prior to the onset of twinning, depending on Sn content and slip mode activities, greatly determines twinning activity.

Acknowledgements

Present work is funded jointly by EPSRC, UK (EP/I012346/1) and Department of Atomic Energy, India, under Indo-UK collaborative programme on “Peaceful uses of Nuclear Energy”.

References

[1] E. Tenckhoff, J. ASTM Int. 2 (2005) 12945.
[2] P. Polukhin, S. Gorelik, V. Vorontsov, Physical Principles of Plastic Deformation, Mir Publication, Moscow, USSR, Moscow, 1983.
[3] J.W. Christian, S. Mahajan, Prog. Mater. Sci. 39 (1995) 1.
[4] H. Abdolvand, M.R. Daymond, C. Mareau, Int. J. Plast. 27 (2011) 1721.
[5] D.G.L. Prakash, R. Ding, R.J. Moat, I. Jones, P.J. Withers, J.Q. Fonseca, M. Da, Preuss, Mater. Sci. Eng. A 527 (2010) 5734.
[6] A. Akhtar, J. Nucl. Mater. 47 (1973) 79.
[7] A. Akhtar, Metall. Mater. Trans. A 6 (1975) 1217.
[8] E. Tenckhoff, Deformation Mechanisms, Texture, and Anisotropy in Zirconium and Zircaloy, in: ASTM STP 966, Philadelphia PA, 1988.
[9] S. Mahajan, D.F. Williams, Int. Met. Rev. 18 (1973) 43.
[10] D. Brown, S. Agnew, M. Bourke, Mater. Sci. Eng. A 399 (2005) 1.
[11] T. Nogaret, W.A. Curtin, J.A. Yasi, L.G. Hector, D.R. Trinkle, Acta Mater. 58 (2010) 4332.
[12] H.A. Khater, D.J. Bacon, Acta Mater. 58 (2010) 2978.
[13] H. Abdolvand, M.R. Daymond, Acta Mater. 60 (2012) 2240.
[14] S. Mendelson, Scr. Metall. 4 (1970) 5.
[15] S. Mendelson, Mater. Sci. Eng. 4 (1969) 231.
[16] J. Wang, J.P. Hirth, C.N. Tomé, Acta Mater. 57 (2009) 5521.
[17] J. Wang, R.G. Hoagland, J.P. Hirth, L. Capolungo, I.J. Beyerlein, C.N. Tomé, Scr. Mater. 61 (2009) 903.
[18] M.H. Yoo, J.R. Morris, K.M. Ho, S.R. Agnew, Metall. Mater. Trans. A 33 (2002) 813.
[19] N. Stanford, M.R. Barnett, Int. J. Plast. 47 (2013) 165.
[20] K.V. Mani Krishna, D.G.L. Prakash, D. Srivastava, N. Saibaba, J. Quinta da Fonseca, G.K. Dey, M. Preuss, J. ASTM Int. 17 (2013) 138–158 (STP 1543).
[21] J.R. Santisteban, M.R. Daymond, J.A. James, L. Edwards, J. Appl. Crystallogr. 39 (2006) 812.
[22] J.R. Santisteban, L. Edwards, A. Steuwer, P.J. Withers, J. Appl. Crystallogr. 34 (2001) 289.
[23] J. Wang, I.J.J. Beyerlein, J.P.P. Hirth, C.N. Tome, C.N. Tomé, Acta Mater. 59 (2011) 3990.
[24] P. Bate, Philos. Trans. R. Soc. A: Math. Phys. Eng. Sci. 357 (1999) 1589.
[25] I.J. Beyerlein, C.N. Tome, R. Proc, A. Soc, Math. Phys. Eng. Sci. 466 (2010) 2517.
[26] C.A. Calhoun, E. Garlea, R.P. Mulay, T.A. Sisneros, S.R. Agnew, Acta Mater. 85 (2015) 168.
[27] C.A. Calhoun, J.A. Wollmershauser, D.W. Brown, E. Garlea, S.R. Agnew, Scr. Mater. 69 (2013) 566.
[28] S.R. MacEven, C.N. Tome, J. Faber, Acta Mater. 37 (1989) 979.
[29] R.A. Holt, M.R. Daymond, F. Xu, S. Cai, J. ASTM Int. 5 (6) (2008) 5.
[30] G. Monnet, B. Devincre, L.P.P Kubin, Acta Mater. 52 (2004) 4317.
[31] R.E. Voskoboinikov, Y.N. Osetsky, D.J. Bacon, Mater. Sci. Eng. A 400–401 (2005) 45.
[32] D.H. Sastry, M.J. Luton, J.J. Jonas, Philos. Mag. 30 (2006) 115.
[33] I.J. Beyerlein, C.N. Tomé, Int. J. Plast. 24 (2008) 867.